

This work was written as part of one of the author's official duties as an Employee of the United States Government and is therefore a work of the United States Government. In accordance with 17 U.S.C. 105, no copyright protection is available for such works under U.S. Law.

Public Domain Mark 1.0

<https://creativecommons.org/publicdomain/mark/1.0/>

Access to this work was provided by the University of Maryland, Baltimore County (UMBC) ScholarWorks@UMBC digital repository on the Maryland Shared Open Access (MD-SOAR) platform.

**Please provide feedback**

Please support the ScholarWorks@UMBC repository by emailing [scholarworks-group@umbc.edu](mailto:scholarworks-group@umbc.edu) and telling us what having access to this work means to you and why it's important to you. Thank you.

# Plasmon resonance-based optical trapping of single and multiple Au nanoparticles

K. C. Toussaint, Jr.,<sup>1</sup> M. Liu,<sup>1,2</sup> M. Pelton,<sup>4</sup> J. Pesic,<sup>1,2</sup> M. J. Guffey,<sup>1,2</sup>  
P. Guyot-Sionnest,<sup>1,2,3</sup> and N. F. Scherer<sup>1,2,4\*</sup>

<sup>1</sup>The James Franck Institute, <sup>2</sup>Department of Chemistry, and <sup>3</sup>Department of Physics,  
The University of Chicago, 929 E. 57th Street, Chicago, Illinois 60637

<sup>4</sup>Center for Nanoscale Materials, Argonne National Laboratory, 9700 S. Cass Ave., Bldg. 440,  
Argonne, Illinois 60439

[nfschere@uchicago.edu](mailto:nfschere@uchicago.edu)

**Abstract:** The plasmon resonance-based optical trapping (PREBOT) method is used to achieve stable trapping of metallic nanoparticles of different shapes and composition, including Au bipyramids and Au/Ag core/shell nanorods. In all cases the longitudinal plasmon mode of these anisotropic particles is used to enhance the gradient force of an optical trap, thereby increasing the strength of the trap potential. Specifically, the trapping laser is slightly detuned to the long-wavelength side of the longitudinal plasmon resonance where the sign of the real component of the polarizability leads to an attractive gradient force. A second (femtosecond pulsed) laser is used to excite two-photon fluorescence for detection of the trapped nanoparticles. Two-photon fluorescence time trajectories are recorded for up to 20 minutes for single and multiple particles in the trap. In the latter case, a stepwise increase reflects sequential loading of single Au bipyramids. The nonlinearity of the amplitude and noise with step number are interpreted as arising from interactions or enhanced local fields amongst the trapped particles and fluctuations in the arrangements thereof.

© 2007 Optical Society of America

**OCIS codes:** (140.7010) Trapping; (240.6680) Surface Plasmons; (180.0180) Microscopy.

---

## References and links

1. A. Ashkin, J. M. Dziedzic, J. E. Bjorkholm, S. Chu, "Observation of a single-beam gradient force optical trap for dielectric particles," *Opt. Lett.* **11**, 288-290 (1986).
2. A. Ashkin, "Optical trapping and manipulation of neutral particles using lasers," *Proc. Natl. Acad. Sci.* **94**, 4853-4860 (1997).
3. A. Ashkin, *Optical trapping and manipulation of neutral particles using lasers*, World Scientific (2006).
4. K. Dholakia and P. Reece, "Optical micromanipulation takes hold," *Nano Today* **1**, 18-27 (2006).
5. D. G. Grier, "A revolution in optical manipulation," *Nature* **424**, 810-816 (2003).
6. G. M. Wang, E. M. Seveck, E. Mittag, D. J. Searles, D. Evans, "Experimental demonstration of violations of the second law of thermodynamics for small systems and short time scales," *Phys. Rev. Lett.* **89**, 050601 (2002).
7. M. D. Wang, J. M. Schnitzer, H. Yin, R. Landick, J. Gelles, S. M. Block, "Force and velocity measured for single molecules of RNA polymerase," *Science* **282**, 902-907 (1998).
8. J. Liphardt, B. Onoa, S. B. Smith, I. Tinoco, Jr., C. Bustamante, "Reversible unfolding of single RNA molecules by mechanical force," *Science* **292**, 733-737 (2001).
9. E. R. Dufresne and D. G. Grier, "Optical tweezer arrays and optical substrates created with diffractive optics," *Rev. Sci. Instrum.* **69**, 1974-1977 (1998).

10. K. C. Neuman and S. M. Block, "Optical trapping," *Rev. Sci. Instrum.* **75**, 2787-2809 (2004).
11. P. A. Prentice, M. P. MacDonald, T. G. Frank, A. Cuschieri, G. C. Spalding, W. Sibbett, P. A. Campbell, K. Dholakia, "Manipulation and filtration of low index particles with holographic Laguerre-Gaussian optical trap arrays," *Opt. Express* **12**, 593-600 (2004).
12. K. Svoboda and S. M. Block, "Optical trapping of metallic Rayleigh particles," *Opt. Lett.* **19**, 930-932 (1994).
13. A. Zelenina, R. Quidant, M. Nieto-Vesperinas, "Enhanced optical forces between coupled resonant metal nanoparticles," *Opt. Lett.* **32**, 1156-1158 (2007).
14. É. Lamothe, G. Lévêque, O. J. F. Martin, "Optical forces in coupled plasmonic nanosystems: near field and far field interaction regimes," *Opt. Express* **15**, 9631-9644 (2007).
15. M. M. Burns, J.-M. Fournier, J. A. Golovchenko, "Optical binding," *Phys. Rev. Lett.* **63**, 1233-1236 (1989).
16. J. Plewa, E. Tanner, D. M. Muth, D. G. Grier, "Processing carbon nanotubes with holographic optical tweezers," *Opt. Express* **12**, 1978-1981 (2004).
17. S. Tan, H. A. Lopez, C. W. Cai, Y. Zhang, "Optical trapping of single-walled carbon nanotubes," *Nano Lett.* **4**, 1415-1419 (2004).
18. R. Agarwal, K. Ladavac, Y. Roichman, G. Yu, C. M. Lieber, D. G. Grier, "Manipulation and assembly of nanowires with holographic optical traps," *Opt. Express* **13**, 8906-8912 (2005).
19. P. M. Hansen, V. K. Bhatia, N. Harrit, L. Oddershede, "Expanding the optical trapping range of gold nanoparticles," *Nano Lett.* **5**, 1937-1942 (2005).
20. J. Prikulis, F. Svedberg, M. Käll, J. Enger, K. Ramser, M. Goksör, D. Hanstorp, "Optical spectroscopy of single trapped metal nanoparticles in solution," *Nano Lett.* **4**, 115-118 (2004).
21. Y. Seol, A. E. Carpenter, T. T. Perkins, "Gold nanoparticles: Enhanced optical trapping and sensitivity coupled with significant heating," *Opt. Lett.* **31**, 2429-2431 (2006).
22. A. Ashkin and J. M. Dziedzic, "Observation of resonances in the radiation pressure on dielectric spheres," *Phys. Rev. Lett.* **38**, 1351-1354 (1977).
23. S. Chu, J. E. Bjorkholm, A. Ashkin, A. Cable, "Experimental observation of optically trapped atoms," *Phys. Rev. Lett.* **57**, 314-317 (1986).
24. R. R. Agayan, F. Gittes, R. Kopelman, C. F. Schmidt, "Optical trapping near resonance absorption," *Appl. Opt.* **41**, 2318-2327 (2002).
25. D. T. Chiu and R. N. Zare, "Biased diffusion, optical trapping, and manipulation of single molecules in solution," *J. Am. Chem. Soc.* **118**, 6512-6513 (1996).
26. M. A. Osborne, S. Balabramanian, W. S. Furey, D. Klenerman, "Optically biased diffusion of single molecules studied by confocal fluorescence microscopy," *J. Phys. Chem. B* **102**, 3160-3167 (1998).
27. T. Iida and H. Ishihara, "Theoretical study of the optical manipulation of semiconductor nanoparticles under an excitonic resonance condition," *Phys. Rev. Lett.* **90**, 057403 (2003).
28. M. Pelton, "Comment on 'Theoretical study of the optical manipulation of semiconductor nanoparticles under an excitonic resonance condition'," *Phys. Rev. Lett.* **92**, 89701 (2004).
29. J. R. Arias-Gonzalez and M. Nieto-Vesperinas, "Optical forces on small particles: attractive and repulsive nature and plasmon-resonance conditions," *J. Opt. Soc. Am. A* **20**, 1201-1209 (2003).
30. A. S. Zelenina, R. Quidant, G. Cadenes, M. Nieto-Vesperinas, "Tunable optical sorting and manipulation of nanoparticles via plasmon excitation," *Opt. Lett.* **31**, 2054-2056 (2006).
31. M. Pelton, M. Liu, S. Park, N. F. Scherer, P. Guyot-Sionnest, "Ultrafast resonant optical scattering from single gold nanorods: large nonlinearities and plasmon saturation," *Phys. Rev. B* **73**, 155419 (2006).
32. C. F. Bohren and D. R. Huffman, *Absorption and Scattering of Light by Small Particles*, John Wiley & Sons (1983).
33. M. Pelton, M. Liu, H. Y. Kim, G. Smith, P. Guyot-Sionnest, N. F. Scherer, "Optical trapping and alignment of single gold nanorods using plasmon resonances," *Opt. Lett.* **31**, 2075-2077 (2006).
34. C. Sönnichsen, T. Franzl, T. Wilk, G. von Plessen, J. Feldmann, O. Wilson, P. Mulvaney, "Drastic reduction of plasmon damping in gold nanorods," *Phys. Rev. Lett.* **88**, 077402 (2002).
35. U. Krebig and M. Volmer, *Optical Properties of Metal Clusters*, Springer (1995).
36. L. Novotny and B. Hecht, *Principles of Nano-Optics*, Cambridge University Press (2006).
37. M. Liu and P. Guyot-Sionnest, "Synthesis and optical characterization of Au/Ag core/shell nanorods," *J. Phys. Chem. B* **108**, 5882-5888 (2004).
38. M. Liu and P. Guyot-Sionnest, "Mechanism of silver(I)-assisted growth of gold nanorods and bipyramids," *J. Phys. Chem. B* **109**, 22192-22200 (2005).
39. R. M. Dickson, D. J. Norris, W. E. Moerner, "Simultaneous imaging of individual molecules aligned both parallel and perpendicular to the optic axis," *Phys. Rev. Lett.* **81**, 5322-5325 (1998).
40. H. Xu and M. Käll, "Surface-plasmon-enhanced optical forces in silver nanoaggregates," *Phys. Rev. Lett.* **89**, 246802 (2002).
41. A. J. Hallock, P. L. Redmond, L. E. Brus, "Optical forces between metallic particles," *Proc. Natl. Acad. Sci.* **102**, 1280-1284 (2005).
42. B. M. Reinhard, M. Siu, H. Agarwal, A. P. Alivisatos, J. Liphardt, "Calibration of dynamic molecular rulers based on plasmon coupling between gold nanoparticles," *Nano Lett.* **5**, 2246-2252 (2005).

43. K. C. Toussaint, Jr., S. Park, J. E. Jureller, N. F. Scherer, "Generation of optical vector beams with a diffractive optical element interferometer," *Opt. Lett.* **30**, 2846-2848 (2005).
44. B. Richards and E. Wolf, "Electromagnetic diffraction in optical systems. II. Structure of the image field in an aplanatic system," *Proc. R. Soc. A.* **253**, 358-379 (1959).

## 1. Introduction

The use of a tightly-focused laser beam to trap and manipulate nanometer to micron-sized particles has become widespread since its inception [1, 2, 3]. Indeed, the optical trapping or "tweezing" of such particles has resulted in new fundamental science and diverse applications in the biological and physical sciences [4, 5], including, the characterization of glassy and nonequilibrium phenomena in colloidal solutions [2, 6], measurement of the forces produced by RNA polymerase during DNA transcription [7], measuring the transition state dynamics of single molecule (RNA) folding [8], and the creation of arbitrary three-dimensional arrays of traps [9].

Optical trapping involves a competition between a "gradient force," which is strongest at the location of maximum gradient of the intensity of a laser beam, and a "scattering force," which results from the radiation pressure that tends to push an object along a beam's propagation direction. Stable trapping occurs when the former is stronger than the latter, which is achieved when the trapping laser light is tightly focused with a high numerical aperture lens [2, 10]. The theory of operation is best described when operating in one of two regimes, either Rayleigh or ray optics. In the latter picture, wherein objects are large compared to the optical wavelength, refraction of the light leads to a momentum recoil that directs them toward the laser intensity maximum [1]. Generally, this is true for objects whose refractive index is larger than that of the surrounding medium, whereas beam shaping has been used to obtain stable trapping when the object's refractive index is smaller [11].

Alternatively, objects in the Rayleigh regime, viewed as induced dipoles upon interaction with an optical field, are small compared to the wavelength of the trapping laser and minimize energy by moving towards the maximum of the intensity. For a monochromatic field  $E$ , of angular frequency,  $\omega$ , the time-averaged optical force acting on a particle in the Rayleigh regime is [12]

$$\langle F \rangle = \frac{\text{Re}[\alpha(\omega)]}{2} \nabla \langle |E|^2 \rangle + \frac{n_m}{c} [\sigma_{\text{abs}} + \sigma_{\text{scatt}}] \langle E \times B \rangle \quad (1)$$

where  $\langle \dots \rangle$  represents the time-average,  $\alpha$  is the frequency-dependent electric polarizability of the particle (and is proportional to its volume),  $B$  is the magnetic component of the input optical field,  $n_m$  is the real-valued index of refraction of the medium,  $c$  is the speed of light in vacuum, and  $\sigma_{\text{abs}}$  and  $\sigma_{\text{scatt}}$  are the absorption and scattering cross-sections, respectively. The first term is conventionally referred to as a gradient force and the second as a scattering force.

The ability to trap and steer nanoparticles of different shapes in three dimensions in solution could be useful in the creation of nanoparticle arrays with novel photonic applications. Furthermore, such a technique could be used to investigate optically-induced electromagnetic interactions between nanoparticles as a function of shape and/or composition [13, 14], analogous to the "optical binding" observed between micron-sized particles [15]. However, Eq. (1) shows why trapping nanometer-sized particles has proved challenging; the gradient force scales as the particle volume and scattering force only as the area (i.e., cross-section). Therefore, the number of experiments that have demonstrated stable, three-dimensional trapping of objects with nanometer-scale dimensions have been limited. For example, objects such as carbon nanotubes [16, 17] and semiconductor nanowires [18] can be trapped because of their micron-scale extension in one dimension. In addition, gold spheres with diameters as small as 20 nm have been trapped by utilizing their large refractive index in the infrared [12, 19], but achieving



stable, three-dimensional trapping is difficult [20], and is accompanied by significant heating [21].

Mitigating these difficulties is possible, enhancing trapping forces while avoiding unacceptable levels of heating, by exploiting optical resonances. As far back as 1977, it was observed that Mie resonances enhance the radiation pressure on optically levitated dielectric spheres [22], and the first experimental report of laser tweezers includes a proposal to use resonances to enhance trapping forces [1]. Shortly afterwards, optical trapping of neutral atoms was demonstrated through careful tuning of laser frequency near atomic transitions [23]. Although theoretical work has developed the idea of resonance enhancement for the room-temperature trapping of particles in solution [24], experimental success has been limited. Resonances have been shown to slow down the diffusion of single molecules in solution [25, 26], and it has been proposed that excitonic transitions in semiconductor nanocrystals could permit their optical trapping [27], but the trapping forces in these cases are limited by the broad linewidths and low saturation intensities of the transitions. Therefore, room-temperature trapping times are limited to a few milliseconds, and stable trapping would require operation at liquid-helium temperatures [28].

Noble metallic nanoparticles, such as gold and silver, are excellent candidates for trapping [29, 30]. They exhibit strong plasmon resonances, associated with the collective oscillation of conduction electrons in the particle, which have very high saturation intensities [31]. In particular, metallic nanorods possess a strong longitudinal-plasmon resonance, corresponding to electron oscillation along the long axis of the rods, whose frequency can be tuned throughout the visible and near-infrared frequency range by controlling the aspect ratio and composition of the rods [32].

Recently, stable trapping of Au nanorods only 40-80 nm in length and 10-15 nm in diameter was accomplished using the near-resonance enhancement of the particle polarizability associated with the plasmon mode [33]. In this paper we further develop this plasmon resonance-based optical trapping (PREBOT) method with independent control of both the trap and probe beams and extend the previous results for Au nanorods to the first demonstration of stable trapping of Au bipyramids and Au/Ag core/shell nanorods. Finally, we show that resonant optical traps can stably hold multiple nanoparticles for periods of minutes. Sequential loading of the trap will allow studying electromagnetic interactions between particles.

## 2. Theory

To further elucidate the operational principle of PREBOT we consider the case of metallic ellipsoids much smaller than the wavelength of the trapping laser. The dipole approximation is a sufficient model for the particle sizes used in our experiments [31, 34]. The large scattering and absorption cross-sections follow from the electric polarizability in the Rayleigh limit, where the polarizability for an ellipsoid with principal axis  $j$  parallel to the direction of polarization of the optical field is [35]

$$\alpha(\omega) = \epsilon_o V \frac{\epsilon(\omega) - \epsilon_m}{\epsilon_m + [\epsilon(\omega) - \epsilon_m] L_j}. \quad (2)$$

Here,  $V$  is the volume of the ellipsoid,  $\epsilon_o$  is the permittivity of free space,  $\epsilon(\omega)$  is the complex dielectric function of the ellipsoid,  $\epsilon_m$  is the dielectric constant of the medium (assumed to be real), and  $L_j$  is a geometrical factor. We model Au nanorods as prolate spheroids where only two of the three principal axes are independent. The frequency-dependent cross-sections for scattering and absorption are [36]

$$\sigma_{scatt}(\omega) = \frac{k^4}{6\pi\epsilon_o^2} |\alpha(\omega)|^2 \quad (3)$$

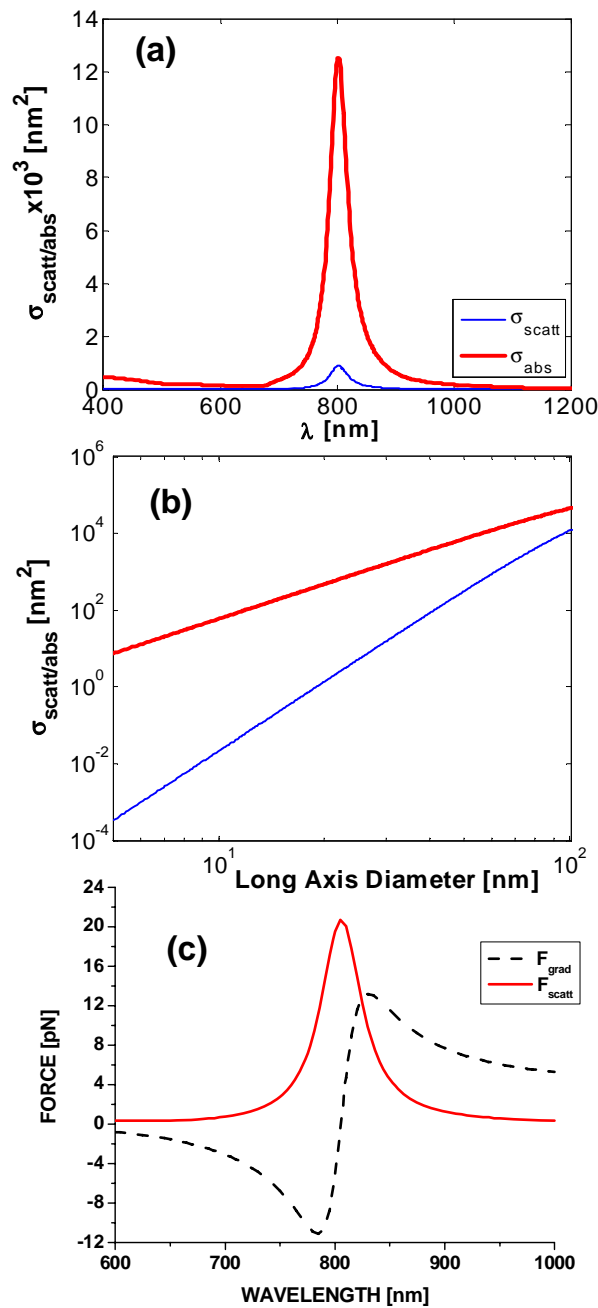


Fig. 1. Simulated: (a) absorption (red curve) and scattering (blue curve) cross-sections for the longitudinal plasmon mode of a single Au nanorod in water with aspect ratio 4.6 (15 nm x 60 nm), (b) difference in magnitude between the cross-sections as the diameter of the long axis of the nanorods increases (and fixed aspect ratio 4.6), and (c) optical gradient force (red curve) and scattering force (black curve) acting on a Au nanorod with aspect ratio 4.6 (15 nm x 60 nm). The model is valid in the dipole limit and assumes that the polarization of the optical field is parallel to the long axis of the rod.

and

$$\sigma_{abs}(\omega) = \frac{k}{\epsilon_o} \text{Im}[\alpha(\omega)] \quad (4)$$

respectively, and  $k$  is the wavevector in the medium. Figure 1(a) shows the scattering and absorption cross-sections for the longitudinal plasmon mode of a Au nanorod with aspect ratio 4.6, and surrounding medium  $\epsilon_m = 1.77$  (water). The resulting plasmon resonance occurs at 800 nm wavelength, and the cross-section for absorption is several times that of scattering. Figure 1(b) is a log-log plot of the scattering and absorption cross-sections for Au nanorods using the long axis length (and fixed aspect ratio of 4.6) up to 100 nm in length. The plasmon resonance remains centered at 800 nm. The magnitude of the gradient and scattering forces acting on a Au nanorod (15 nm diameter and 60 nm length) resulting from a 100 mW beam that is focused to a diffraction-limited spot is shown in Fig. 1(c). The gradient force is significantly increased when the trap laser wavelength is detuned to the long-wavelength side of the longitudinal plasmon resonance. An optimal detuning for Au nanorods is approximately 50 nm, where PREBOT achieves a trap potential depth of several  $k_b T$  ( $k_b T = 4 pN \cdot nm$ ).

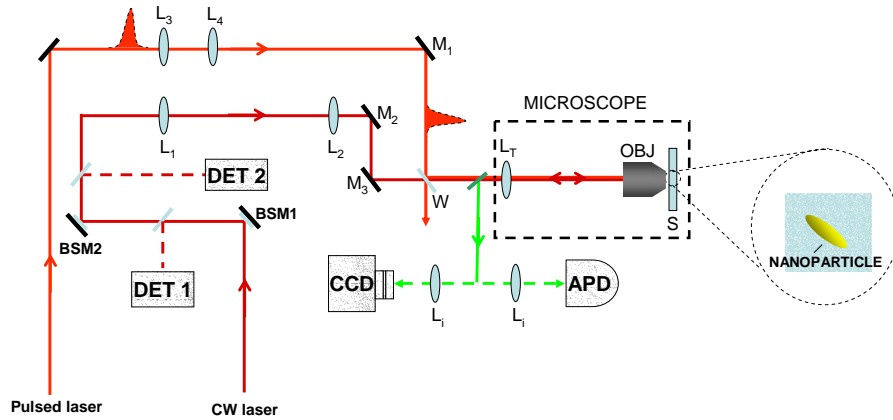


Fig. 2. PREBOT setup. Two lasers are used; one for trapping (solid red line) and one for probing (dashed orange line) of sample. The beam path used for trapping consists of lenses  $L_1$  and  $L_2$  of focal lengths 20 cm and 25 cm, respectively, and steering mirrors  $M_2$  and  $M_3$ . Beam-pointing stability is maintained through the use of beam stabilizing mirrors ( $BSM_1$  and  $BSM_2$ ) and position-sensitive photodiodes ( $DET_1$  and  $DET_2$ ). The probe beam path has lenses  $L_3$  and  $L_4$  of equal focal length 5 cm, and steering mirror  $M_1$ . The beams are spatially combined at window  $W$  before entering the microscope.  $L_T$  is a tube lens of focal length 20 cm, and  $OBJ$  and  $S$  represent the water-immersion objective lens and sample, respectively. Two-photon fluorescence (green) is imaged using  $L_i$  to either a CCD camera or APD detector. The polarization of the probe beam is kept linear. The power of the trap beam was kept constant at approximately 100 mW at the input to the microscope (with  $\sim 60$  mW delivered to the sample) for all experiments reported here; the probe beam power was also kept constant at approximately 10 mW at the input to the microscope (with  $\sim 6$  mW delivered to the sample).

### 3. Experiment

Figure 2 is a schematic of the PREBOT setup. The trapping beam is obtained from a tunable, continuous-wave, linearly polarized Ti:Sapphire laser (Coherent). The beam is sent through a telescope (lenses  $L_1$  and  $L_2$ ), a tube lens,  $L_T$ , and into an inverted microscope (Nikon). The telescope focal lengths are chosen such that the beam diameter at the back focal plane of the microscope's water-immersion objective lens (Olympus UPLSAPO 60X 1.2 NA) is approximately 1 cm. The probe beam, derived from a pulsed and tunable Ti:Sapphire laser (Spectra-Physics Mai Tai) that produces sub-100 femtosecond-duration pulses at 80 MHz repetition rate, travels along a parallel path. The probe laser is tunable from 800 to 880 nm; the wavelength chosen depends on the ensemble spectra of the samples. The probe pulses are linearly polarized and spectrally centered at 800 nm for the experiments reported here. Dispersion to be encountered is pre-compensated by double passing a prism pair. The pulses travel through a 1:1 telescope (lenses  $L_3$  and  $L_4$ ) before being combined with the trap beam via a first surface reflection from a 1-inch diameter BK7 window. This configuration allows independent focus control of the trap and probe beams, which is essential for optimizing signal detection from trapped nanoparticles. The pulses are focused into the sample by the same microscope objective. A solution of nanoparticles is applied to a standard microscope coverslip (.17 mm thickness), and the microscope objective is adjusted to focus slightly above the coverslip surface. The emitted two-photon fluorescence from the sample is epi-detected, spectrally filtered and imaged onto either a thermoelectrically-cooled CCD (Andor, IXON 887) detector or a photon-counting avalanche photodiode (Perkin-Elmer, SPCM-AQR-15) via lens  $L_i$ .

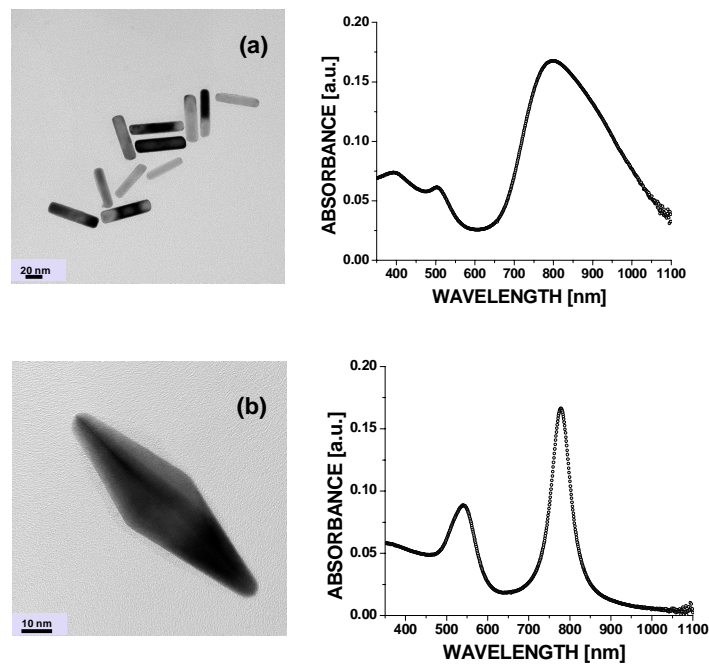


Fig. 3. TEM images and associated ensemble absorption spectra for (a) Au/Ag core/shell nanorods and (b) Au bipyramids in water. The scale bars are (a) 20 nm and (b) 10 nm, respectively.

#### 4. Results and Discussion

We used published methods to chemically synthesize the various types of nanoparticles [37, 38], whose aspect ratios were adjusted such that their longitudinal plasmon resonances are close to 800 nm. The nanoparticles are in aqueous solutions. The solutions contain CTAB (cetyltrimethylammonium bromide), which is a surfactant. For the Au/Ag core/shell nanorods, the solution also contains PVP (polyvinylpyrrolidone). The aspect ratio of the nanorods has a standard deviation of  $\sim 25\%$  (volume has a standard deviation of  $\sim 30\%$ ). All sample concentrations were adjusted such that the arrival rate of the particles in the laser focus is very slow (approximately 1 particle every 10 sec), and the probability of more than one particle arriving at a time is vanishingly small [33]. The Au/Ag core/shell nanorods are 60 nm long with 13 nm diameter and have a shell thickness of 2 nm and (ensemble) linewidth of 180 nm, while the Au bipyramids are 100 nm long and 30 nm diameter. TEM images and associated ensemble absorption spectra for the particle types are shown in Fig. 3. The rods and bipyramids have crystalline order, which is observed at higher magnification [37, 38]. Representative time traces, termed

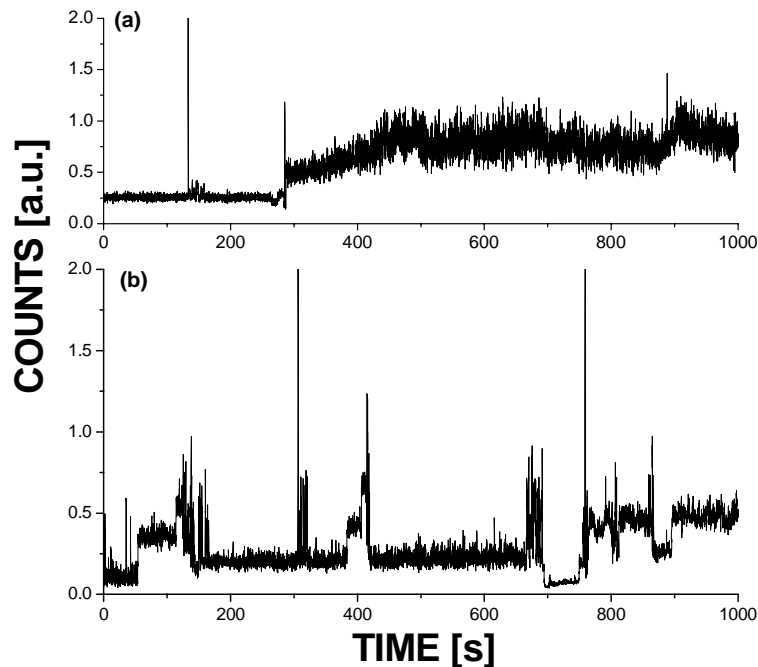


Fig. 4. Two-photon fluorescence time trajectories acquired for (a) Au/Ag core/shell nanorods, and (b) Au bipyramids integrating over  $36 \times 40$  pixels and  $66 \times 60$  pixels of the CCD, respectively. The slow drift in the fluorescence signal is attributed to the relative pointing instability of the trap and probe beams, which causes the axial location of the trap to change with respect to the probe beam focus. The instability is more severe for the Au/Ag particles since they are more difficult to trap due to their broad linewidths.

trapping trajectories, of Au bipyramids and Au/Ag core/shell nanorod samples are shown in Fig. 4. All the particle types studied here are aligned in the optical trap due to their anisotropy in shape and optical resonance [33]. The CCD detector was used to record two-photon fluorescence time trajectories for 10,000 frames and 100 ms exposure time. In the case of the Au bipyramids, the trapping laser is tuned to 850 nm to optimize the trapping on the red side of the

plasmon resonance shown in Fig. 1(c) [33], while the broader linewidth of the Au/Ag core/shell nanorods requires tuning the trapping laser to 880 nm.

The two-photon fluorescence trajectory for a trapped Au/Ag core/shell nanorod sample is shown in Fig. 4(a). During the first few hundred seconds nothing enters the trap and we only record detector readout noise. Shortly before 300 sec a nanorod enters and remains in the trap for the remainder of the time trace. The spikes in the trajectories are typically observed when a particle enters or escapes the trap or if another object briefly passes through the focus. Also, the signal emitted by a single Au/Ag core/shell nanorod is unpolarized as determined by rotating a polarization analyzer placed before the APD, as expected for two-photon fluorescence.

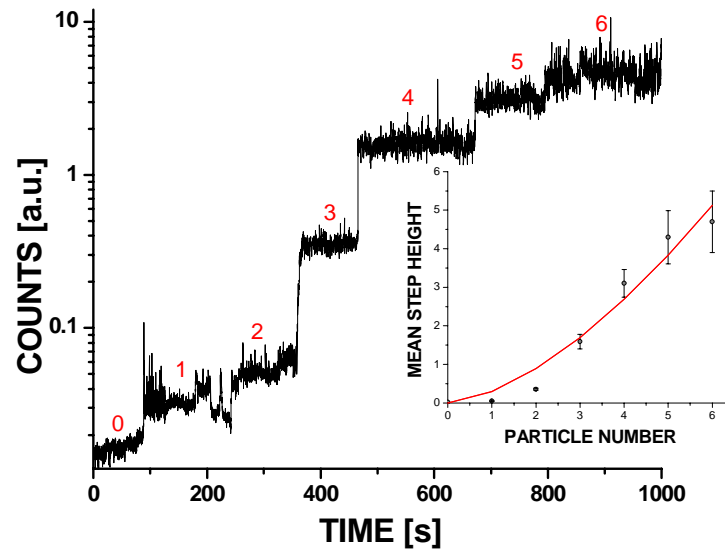


Fig. 5. Time trace showing loading of Au bipyramids integrating over 66 x 60 pixels of the CCD. The numbers 0-6 label the stepwise signal level changes that occur as particles are progressively loaded into the trap. The inset is a linear-linear plot of the mean step height versus particle number with a fit to a polynomial  $y \sim x^n$ ;  $n = 1.6$  (solid red line). The mean value for steps 0-6 are 0.017, 0.050, 0.356, 1.60, 3.10, 4.30, and 4.70, respectively, while the error bars represent the associated standard deviation for each step.

Figure 4(b) shows a two-photon fluorescence trajectory of trapped Au bipyramids. A single particle enters the trap at  $\sim 50$  sec followed by a second particle at 125 sec. The fact that the signal intensity is not simply doubled by the addition of the second particle is probably because the latter is not identical to the first. Subsequently, one of the particles escapes the trap (most likely the first one that had originally entered) at  $\sim 150$  sec, leaving a single particle in the trap until  $\sim 400$  sec whereupon several particles enter the trap in quick succession and all but one leave at 425 sec. Other trapping conditions such as greater trap laser power or lower particle concentration give trajectories of single particles stably trapped for  $> 10$  min.

Assuming that a single step or plateau in a two-photon fluorescence time trajectory is equivalent to 1 particle in the trap, Fig. 5 shows a uniquely informative trajectory of sequential loading of Au bipyramids. We observe six distinct steps or plateaus (labeled 1-6), relative to the baseline (labeled 0), of sequential particle addition. The signal appears to increase nonlinearly

with particle number, rather than the linear dependence expected for independent particles. The inset is a plot of the mean value of each step height versus the particle number. The error bars indicate the increasing standard deviation with particle number.

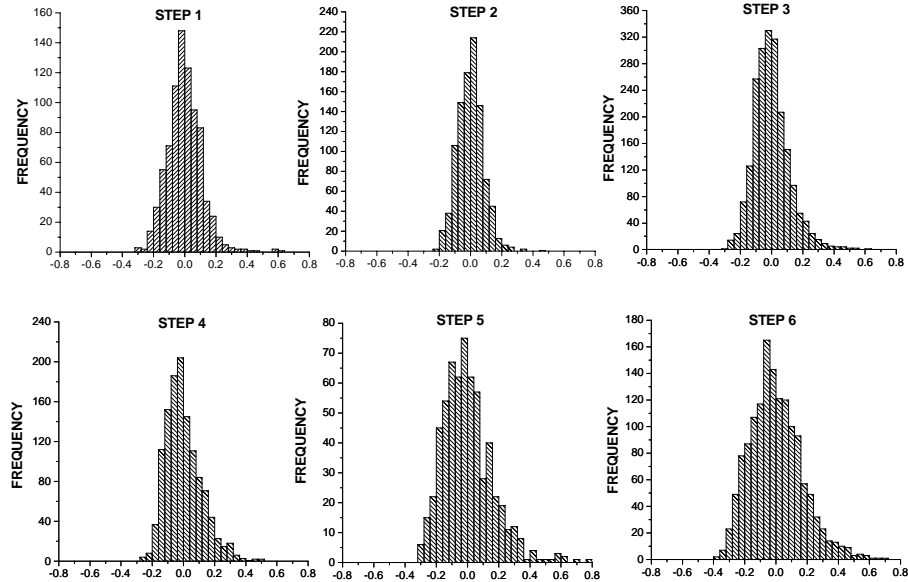


Fig. 6. Histograms of instantaneous signals of Fig. 5 normalized to the mean values. Each distribution corresponds to the associated step number (and mean value) in Fig. 5.

Figure 6 gives the distributions of signal intensity (fluctuations) associated with each step in Fig. 5. Specifically, the values are the instantaneous deviations divided by the mean values for steps 1-6 shown in Fig. 5. The histograms exhibit a positive skew, especially for steps 3-6. Furthermore, unlike the expected Poisson statistical behavior, the noise in the two-photon fluorescence signal is increasing faster than the mean values. Table 1 summarizes the normalized variance for each histogram. The variance for step 0 (i.e., the normalized detection noise) is included for reference.

Figure 7(a) is a series of (intensity normalized) frames of a movie showing the effect of single particles entering the trap, where each panel corresponds to a step (1-6) from Fig. 5. The movie is shown in Fig. 8. There are two interesting features to note. The first is that the diameter of the spot increases with each step. The second is that there is a slight “dip” in intensity near the center of the spot in the fifth panel. These features are more clearly seen in the radial profile plots of Fig. 7(b). The emergence of an apparent Airy disc has been previously observed for slightly defocused images of single emitters [39]. We believe that these unusual features are due to specific geometrical configurations that the multiple particles take while in the trap. We are currently pursuing further studies to understand this behavior.

We assume that the nonlinear dependence of the total two-photon fluorescence signal on particle number in Fig. 5 arises from inter-particle interactions [40, 41]. Finite difference time domain simulations (M.L., P.G.S. unpublished results) indicate that field enhancements extend to lateral distances as large as 50 nm from the center of the bipyramid. Therefore, proximity of particles would allow mutual field enhancements. Furthermore, since the minimum signal



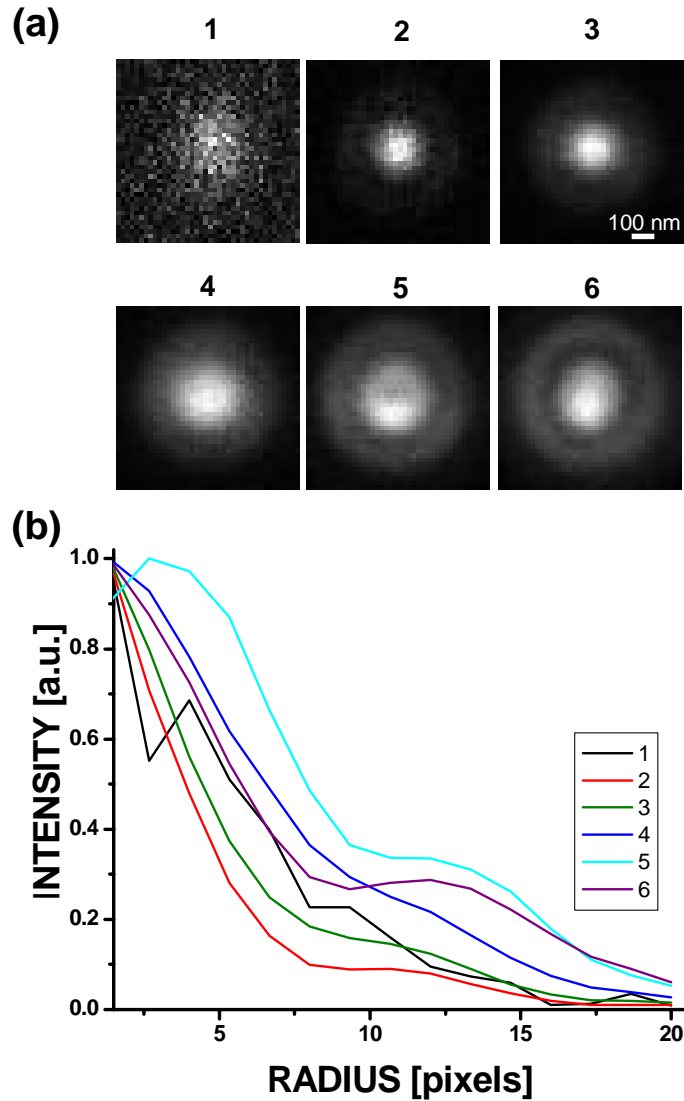


Fig. 7. (a) Sequential frames of a movie (100 ms integration time) of a particle entering the trap integrating over  $40 \times 40$  pixels of the CCD. Each panel is intensity autoscaled and the panel number corresponds to each step in Fig. 5. (b) The associated radial profile plots (normalized to peak intensity). Note that the black curve in (b), corresponding to the first frame in (a), has a background contribution that is not insignificant in comparison to the signal from the particle.

Table 1. Table of two-photon fluorescence normalized variance per step height for the histograms in Fig. 6. We define this normalized variance as the raw variance divided by the mean value of each step.

STEP	Normalized Variance
0	0.023
1	0.009
2	0.006
3	0.009
4	0.010
5	0.020
6	0.026

is that of independent particles, position or configurational fluctuations that give local field enhancements would increase the total (instantaneous) signal, thereby giving a skew to positive signal values.

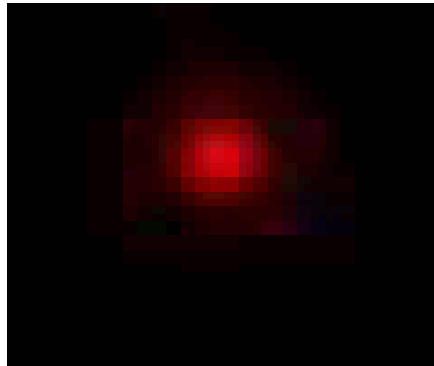


Fig. 8. Movie of multi-particle trapping integrating over 60 x 50 pixels of the CCD.

The stable trapping of multiple single particles also implies limits and constraints on possible plasmonic or photonic (i.e., scattering force) interactions [41]. A strong (axial) inter-particle interaction would result in a large (red) shifted collective plasmon resonance [42] that could cause the particles to leave the trap. Conversely, a laterally disposed arrangement could result in a blue shift (i.e., parallel dipoles), which is not incompatible with the PREBOT effect [see Fig. 1(c)] if the interaction and spectral shift are small (e.g., < 10 nm). The good stability of multiple particles in the trap (e.g., steps 4 and 6 are each 3 minutes long) suggests that the plasmonic interactions and spectral shifts are of order 10 nm or less. Measurements of spectral shifts to quantify these interactions are currently in progress.

Finally, although the power density of the cw trapping laser is  $\sim 10^8$  W/cm<sup>2</sup> we do not see evidence of particle melting or aggregation. Particle melting would result in a significant blue shift ( $\sim 100$  nm) of the longitudinal plasmon resonance [31] thereby weakening the PREBOT effect and ultimately resulting in the particle leaving the trap. Similarly the sequentially loaded

trap does not form an aggregate of bipyramids since their very close proximity as an aggregate would lead to a significant shift of the plasmon resonance (particularly if they are touching or fused) and again would diminish the PREBOT effect causing the particles to rapidly leave the trap [42]. We believe that the particles are kept apart due to both the “repulsive” interaction of aligned dipoles that would occur at close separations and the scattering of photons between particles, the latter being effective on  $\sim 100$  nm length scales [41]. Actually, repulsive interactions would be the critical element in allowing the multiple particles in a single trap to achieve some degree of spatial ordering that could explain the images in Fig. 7.

## 5. Conclusion

PREBOT holds promise for various applications including guided fabrication of ordered arrays of nanoparticles, manipulation of plasmonic nanoparticles in complex environments (e.g., cells), and provides a testbed for studying field-induced inter-particle interactions. The present paper used the PREBOT technique to demonstrate stable trapping of metallic particles of different shapes, such as Au bipyramids, and composition like Au/Ag core/shell nanorods. Stable trapping of multiple particles was achieved in the case of the bipyramids, which have narrow intrinsic plasmon linewidths and small inhomogeneous broadening. The associated two-photon fluorescence signal’s apparent nonlinear dependence with particle number for the case of sequential particle loading, affords qualitative insight into inter-particle interactions. Further studies are in progress to understand this nonlinear behavior as well as investigating trapping as a function of different polarization states of the laser. A cylindrically-symmetric trap potential is expected using circularly polarized light or a radially polarized vector beam [43]. Both would result in tighter focusing and hence increased trapping stability compared to the conventional scalar (i.e., linearly polarized) beam and the associated asymmetric focusing [44].

## Acknowledgments

The submitted manuscript has been created by UChicago Argonne, LLC, Operator of Argonne National Laboratory (“Argonne”). Argonne, a U.S. Department of Energy Office of Science laboratory, is operated under Contract No. DE-AC02-06CH11357. The U.S. Government retains for itself, and others acting on its behalf, a paid-up nonexclusive, irrevocable worldwide license in said article to reproduce, prepare derivative works, distribute copies to the public, and perform publicly and display publicly, by or on behalf of the Government.

We thank Professor Aaron Dinner for insightful conversations. This work was supported by the NSF (CHE-0616663). K. C. T. acknowledges support from the National Science Foundation (DBI-0511849). M.P. and N.F.S. acknowledge the Center for Nanoscale Materials, which is supported by the U. S. Department of Energy, Office of Science, Office of Basic Energy Sciences, under Contract No. DE-AC02-06CH11357. N.F.S. acknowledges the John S. Guggenheim Foundation for a fellowship.